# A New Look at the Melting Layer

FIONA J. DRUMMOND, R. R. ROGERS, AND S. A. COHN

*Atmospheric and Oceanic Sciences, McGill University, Montreal, Quebec, Canada*

W. L. ECKLUND

*Cooperative Institute for Research in Environmental Sciences, University of Colorado/NOAA, Boulder, Colorado*

D. A. CARTER

*NOAA/Aeronomy Laboratory, Boulder, Colorado*

J. S. WILSON

*Cooperative Institute for Research in Environmental Sciences, University of Colorado/NOAA, Boulder, Colorado*

(Manuscript received 24 March 1995, in final form 19 September 1995)

ABSTRACT

The authors derive a relationship between the vertical Doppler spectrum of the rain just below the radar bright band and that of the snow just above. It neglects vertical air motions and assumes that each snowflake simply melts to form a raindrop of the same mass, disregarding other possible effects such as aggregation to form larger particles or breakup to create smaller ones. The relationship shows that, regardless of the dependence of particle fallspeed on size, the product of the equivalent reflectivity factor and the mean Doppler velocity of the snow is proportional to the same product for the rain, with a constant proportionality factor of 0.23, which equals the ratio of the dielectric factors of ice and water. Observed values of the reflectivity and mean Doppler velocity above and below the melting layer sometimes agree with this theoretical prediction but more often deviate from it in ways that may be interpreted as indicating the predominance of either aggregation or breakup processes. The data suggest that aggregation is occurring much of the time in the melting layer but that breakup effects become dominant in heavy precipitation. The analysis is extended by assuming relations between particle size and fallspeed for rain and snow. This enables the comparison of measured spectra with those derived theoretically. A simple allowance for aggregation or breakup in the spectral transformation from snow to rain is found to give improved spectral agreement in cases where these effects are indicated.

## 1. Introduction

In a review of the contributions of radar to precipitation physics, Dennis and Hitschfeld (1990) explain that studies of the bright band associated with the melting level of snow go back to 1946 and thus are as old as radar meteorology itself. An early quantitative study that set the course of much later research is that of Austin and Bemis (1950), who showed that the main features of the reflectivity profile through the melting layer could be explained by aggregation of snowflakes in the brightband region and the increase in fall velocity and the change in the index of refraction of the particles as the snowflakes melt to become raindrops. The trend over the years has been to attribute more and more significance to the melting layer. Not only might it be a favored region for precipitation "enhancement," but the local chilling of the air caused by melting might have important dynamic effects on the convective scale and even the mesoscale. A recent definitive study of the melting layer is that of Willis and Heymsfield (1989), who also review the recent history of the subject. Their work, based on a spiral descent through a melting layer by an airplane equipped with cloud physics instruments and radar, indicated that melting begins above the bright band, causing some particles to fall faster than others and thus leading to aggregation. The reflectivity maximum is explained by a few very large aggregates that survive to temperatures a little warmer than 0°C. Their data also showed evidence of the formation of small crystals by fragmentation processes above the melting layer. Separate from this kind of detailed microphysical study, there have been attempts to develop empirical models of reflectivity profiles

*Corresponding author address:* Dr. R. R. Rogers, Atmospheric Sciences, McGill University, 805 Sherbrooke St. W., Montreal H3A 2K6, PQ, Canada.
E-mail: rogers@zepher.meteo.mcgill.ca

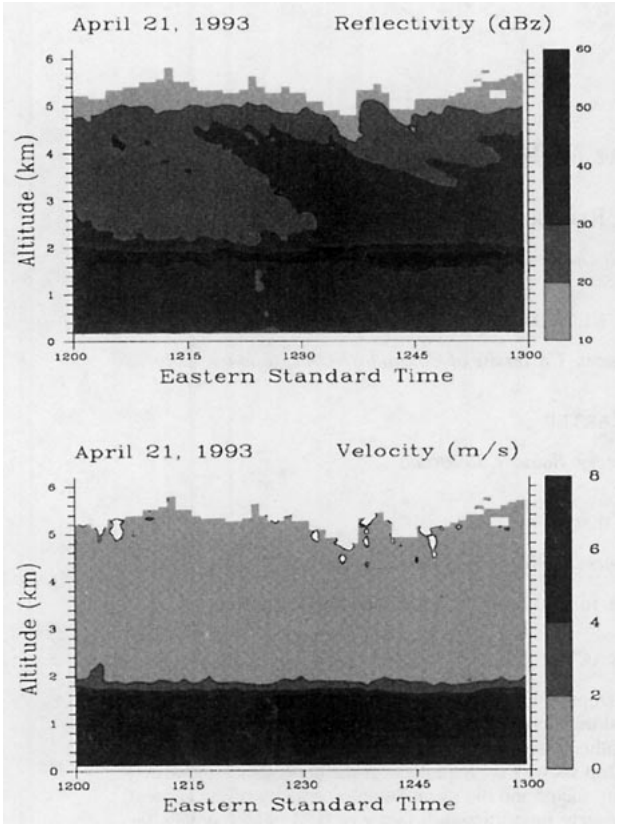


FIG. 1. Time–height patterns of reflectivity factor (above) and mean downward Doppler velocity (below) for case 1.

through the melting layer as a function of the precipitation intensity (e.g., Klaassen 1988). Such models are used to assess the effects of the melting layer on radio propagation over earth–space paths and to estimate the errors caused by the bright band in radar measurements of areal rainfall.

A continuing question since the earliest studies of the melting layer has been how important is aggregation during the conversion from snow to rain. This process seems to be necessary to explain the observed excess reflectivity of the bright band and would account for the existence of larger drops below the melting layer than implied by the snowflakes above. On the other hand, Gunn and Marshall (1958) reported observations in which the size distribution of aggregate snowflakes just prior to melting contained more large particles and fewer small ones than found in the drop size distribution of rain having the same precipitation rate, and concluded that breakup of the snowflakes during melting was important in shaping the raindrop size distribution. Thus, both aggregation and breakup may be occurring in the melting layer, and one may be more important than the other, depending on circumstances.

In this paper, an abridged and revised version of Drummond (1994), we begin with the hypothesis, following Ekpenyong and Srivastava (1970), that there is a one-to-one relationship between the snowflakes entering the melting layer and the raindrops leaving it: there is no aggregation to form larger particles and no breakup to form smaller ones. Furthermore, there is no growth by condensation of vapor or accretion of cloud droplets, so that a snowflake of a given mass becomes a raindrop of the same mass. These assumptions, though at variance with many reported observations, make a good starting point because they lead to a simple relationship between the Doppler spectrum of the snow and that of the rain. We then compare Doppler radar observations above and below the melting layer with the predicted relationship. Although the observations sometimes agree closely with the simple theory, there are often significant differences. The differences may be interpreted as indicating whether aggregation or breakup was the dominant process in the transition from snow to rain. Our data indicate that aggregation prevails much of the time but that breakup tends to dominate when the reflectivity is high.

## 2. Doppler spectra of rain and snow

Let the Doppler spectrum of the rain, normalized to unit area and observed in a vertically pointing beam, be denoted by $S_R(v_R)$, where $v_R$ is the downward velocity of the raindrops. Neglecting vertical air motions, the spectrum is related to the drop size distribution $N_R(D)$ by

$$S_R(v_R) = \frac{\pi^5}{\lambda^4} \frac{|K_R|^2}{\eta_R} N_R(D) D^6 \frac{dD}{dv_R}, \qquad (1)$$

where $\lambda$ is the wavelength, $|K_R|^2$ the dielectric factor for water (numerically, 0.93), and $\eta_R$ the radar reflectivity of the rain.

We assume that each raindrop was created by the melting of a snowflake of the same mass. Thus, there is no breakup, aggregation, or growth of the precipitation particles as they melt. Further, if there is a steady supply of snowflakes above the melting layer, the snowflake size distribution, in terms of melted diameter, is related to that of the raindrops by

$$N_S(D) = \frac{v_R(D)}{v_S(D)} N_R(D), \qquad (2)$$

where $v_R/v_S$, the ratio of the fallspeed of a raindrop to that of a snowflake of the same mass, is a stretching factor to allow for the reduction in the concentration of the precipitation particles as they speed up when melting. It follows from (2) that the precipitation rate in the rain equals that in the snow, as was assumed by Austin and Bemis (1950).

The Doppler spectrum of the snow, normalized to unit area and expressed in terms of melted diameter, may be written

$$S_S(v_S) = \frac{\pi^5}{\lambda^4} \frac{|K_S|^2}{\eta_S} N_S(D) D^6 \frac{dD}{dv_S}, \qquad (3)$$

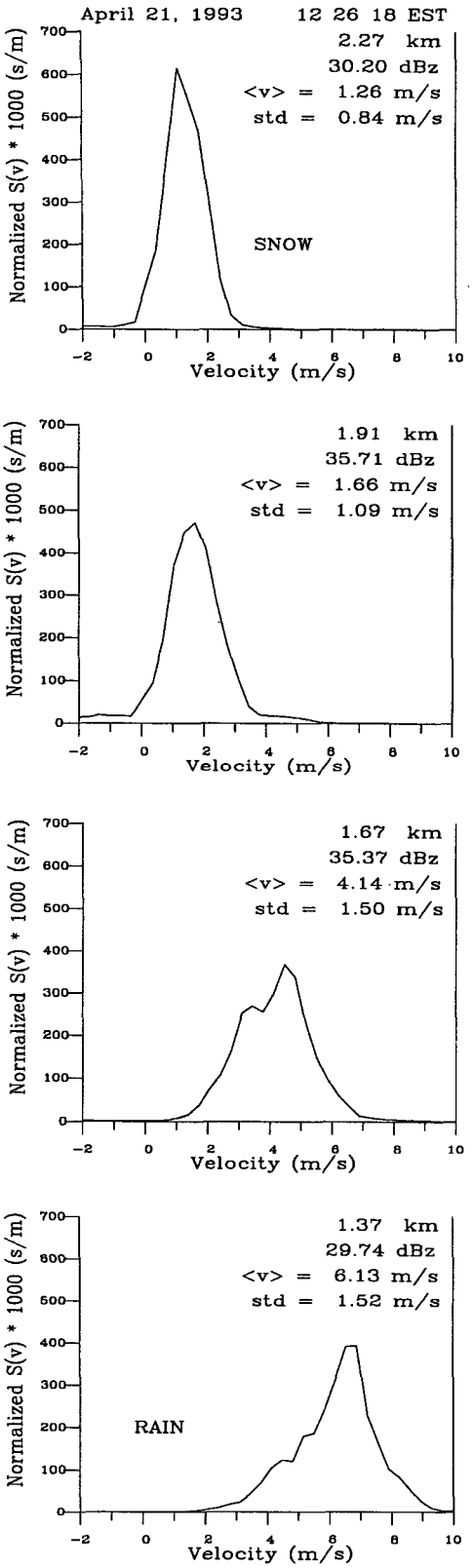


FIG. 2. Doppler spectra at selected altitudes at 1226 EST from case 1, showing the transition from snow to rain. Data in each frame indicate altitude, equivalent reflectivity factor, mean downward velocity, and standard deviation of the spectrum. Sign convention is that precipitation fallspeed (downward Doppler velocity) is positive. Spectral resolution is 0.34 m $s^{-1}$.

where $\eta_S$ is the reflectivity of the snow and $|K_S|^2$ the dielectric factor of ice (effectively 0.21 when size is expressed as melted diameter; see Smith 1984). From (1) and (2), (3) becomes

$$S_S(v_S) = \frac{\eta_R}{\eta_S}\,\mu\,\frac{v_R}{v_S}\,S_R(v_R)\,\frac{dv_R}{dv_S},$$

where $\mu = |K_S|^2/|K_R|^2 = 0.23$. Now, we introduce the reflectivity factors of the rain and the snow by noting that $\eta_R = kZe_R$ and $\eta_S = kZe_S$, where $Ze_R$ is the equivalent reflectivity factor of the rain, $Ze_S$ is the equivalent reflectivity factor of the snow, and $k = \pi^5|K_R|^2\lambda^{-4}$. Thus,

$$S_S(v_S) = \frac{Ze_R}{Ze_S}\,\mu\,\frac{v_R}{v_S}\,S_R(v_R)\,\frac{dv_R}{dv_S} \tag{4}$$

expresses the Doppler spectrum of snow as a function of the Doppler spectrum of the rain it produces. To apply this equation requires knowing the dependence of $v_R$ on $v_S$, which is determined by the relationships between particle fallspeed and size for the rain and for the snow. Note, however, that separating the variables in (4) and integrating over velocity shows that, independently of the relations between particle size and fallspeed,

$$Ze_S\langle v_S\rangle = \mu Ze_R\langle v_R\rangle, \tag{5}$$

where $\langle v_S\rangle$ and $\langle v_R\rangle$ denote the mean Doppler fall velocities in the snow and rain spectra. Thus, in a steady-state melting layer in which vertical air motions are negligible compared with the average particle fallspeed and in which each snowflake melts to produce a raindrop of the same mass, the reflectivities and mean Doppler velocities are related by (5). Typical values of mean velocities are $\langle v_S\rangle \approx 1.5$ m $s^{-1}$ and $\langle v_R\rangle \approx 6$ m $s^{-1}$, so the reflectivity ratio given by (5) is approximately

$$\frac{Ze_S}{Ze_R} = \mu\,\frac{6}{1.5} \approx 1.$$

Empirical models of reflectivity profiles through the melting layer (Klaassen 1988; Fabry and Zawadzki 1995) show about the same reflectivity at the top and bottom of the bright band, especially for low values of precipitation intensity, rainfall rates less than about 1 mm $h^{-1}$. This feature of the models is therefore consistent with the hypothesis of no breakup or aggregation, which leads to the near equivalence of reflectivi-

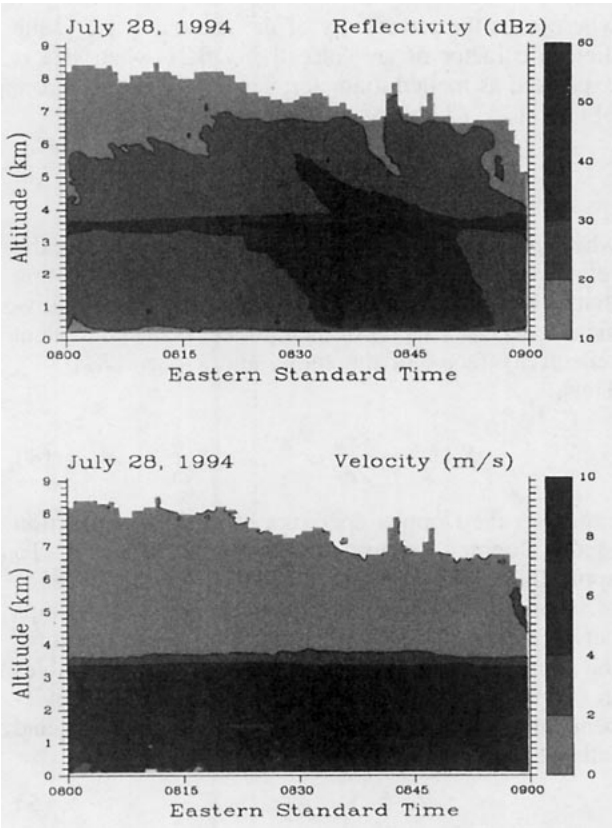


FIG. 3. Time–height patterns of reflectivity (above) and mean downward velocity (below) for case 2.

ties above and below the melting layer because of the coincidence that $\mu = |K_S|^2/|K_R|^2 \approx \langle v_S \rangle / \langle v_R \rangle$. To give credit where credit is due, we acknowledge that Ryde (1946) in his classic paper noted the coincidence that the change in dielectric factor approximately compensates for the increase in fall velocity. What is new in our analysis is (5), which enables a quantitative assessment of the effect through the mean Doppler velocity.

## 3. The observations

The data used in this study are from archival records of the McGill/National Oceanic and Atmospheric Administration boundary layer wind profiler (Rogers et al. 1994). This is a small UHF radar employing a phased array antenna that produces five beams: vertical and 21° off the vertical in the N, S, E, and W directions. The antenna cycles through all or part of these directions sequentially, with the dwell time in each direction usually set to about 30 s, during which there is both coherent (time domain) and incoherent (frequency domain) signal integration. The records consist of average Doppler spectra from as many as 100 ranges in each of the pointing directions, from which can be calculated vertical profiles of the horizontal wind, the reflectivity, the mean Doppler velocity, or other properties of the Doppler spectra.

The first example (case 1) is from 21 April 1993. It was selected for analysis because it is typical of a strong, fairly steady melting layer and because of the high resolution of the observations in time and height. Only the vertical, east, and north beams were used, and the scanning cycle was V-E-V-N. The dwell time at each direction was approximately 30 s, so a complete cycle required 2 min, and the frequency of measurements in the vertical was once a minute. The radar was operating in short-pulse mode (0.4 $\mu$s), and the range resolution was 60 m. Figure 1 shows the (rain equivalent) reflectivity factor and the mean downward velocity in the vertical beam over the period analyzed. The melting layer, just below 2 km, is defined by reflectivities exceeding 40 dBZ and a strong gradient in the downward velocity. A snow trail of higher reflectivity is evident midway through the record. Figure 2 is an example of Doppler spectra measured at different levels at the same time, showing the transition from snow to rain.

Figure 3 shows the second example chosen for analysis, another strong melting layer. As in Fig. 1, peak reflectivities exceed 50 dBZ. Some of the downward

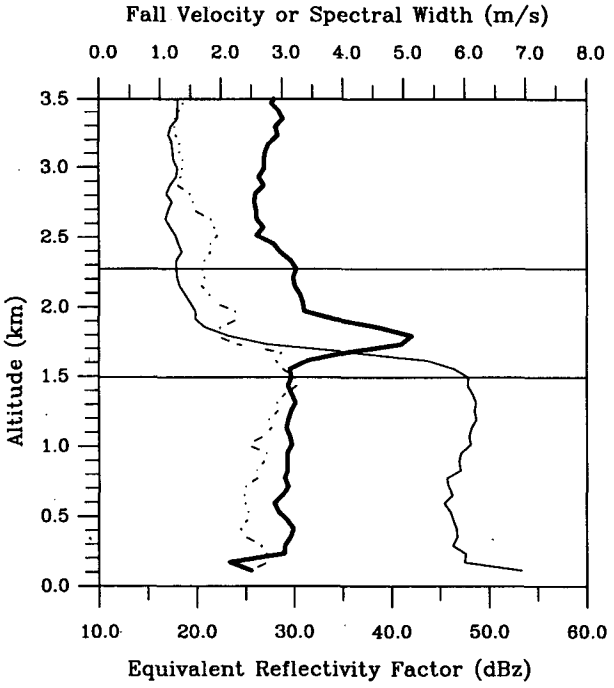


FIG. 4. Vertical profiles of reflectivity (bold), mean downward velocity (solid), and Doppler spectral width (dashed) at 1226 EST in case 1. The melting layer is indicated by reflectivity maximum and strong vertical gradient of mean velocity. The lines drawn at 1.5 and 2.3 km are, respectively, the rain and snow levels identified by the algorithm. The prominent level of maximum curvature just above the brightband peak is rejected by the algorithm because it is within 200 m of the peak.

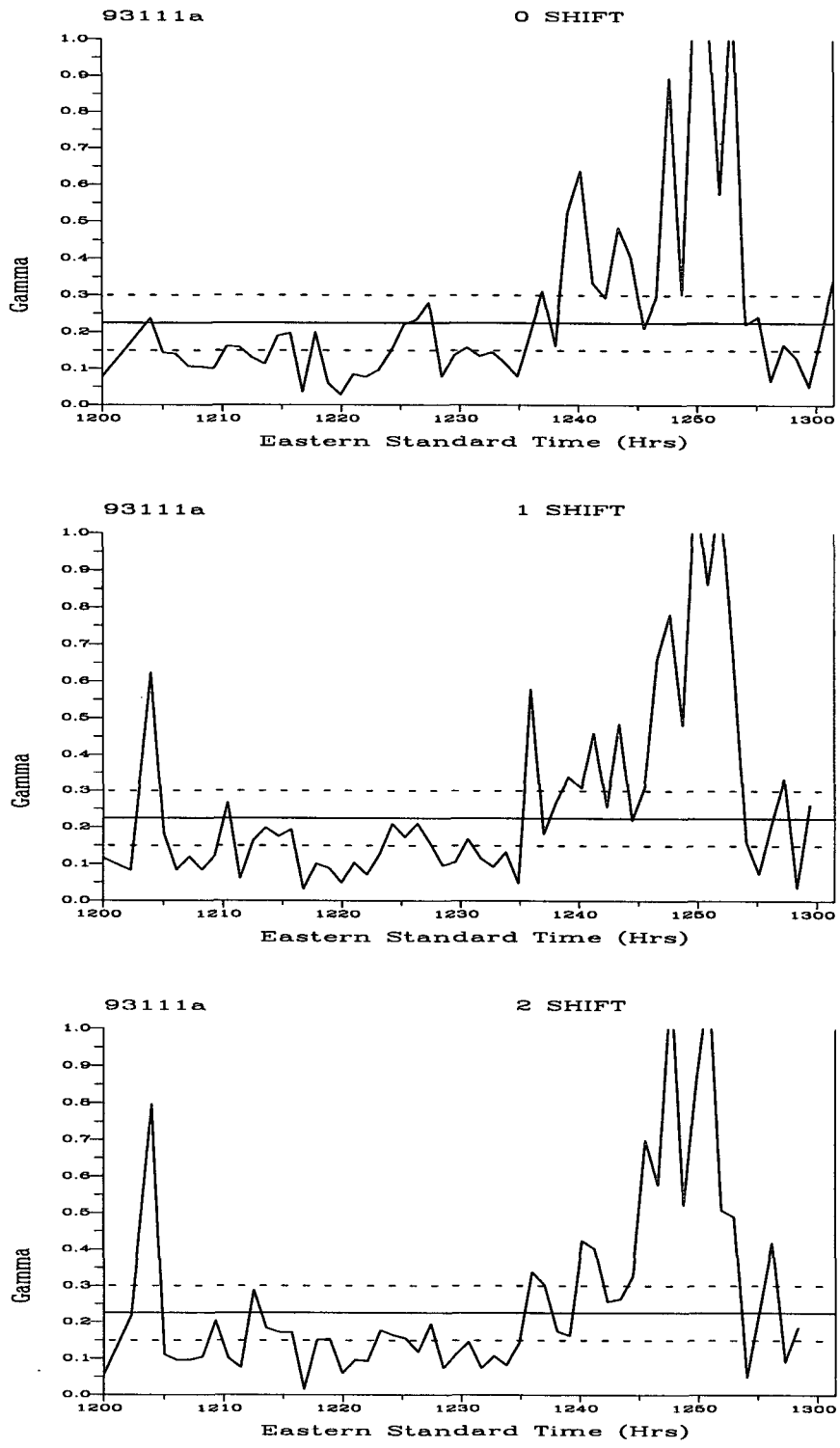


FIG. 5. The parameter $\gamma$ as a function of time for case 1. The top plot (labeled 0 SHIFT) is based on simultaneous measurements in the rain and snow. The middle plot is based on a comparison of the rain record with snow 1 min earlier; the bottom plot is based on a 2-min displacement of the records. A solid line indicates the theoretical value of $\gamma = \mu = 0.23$. Dashed lines define an interval of uncertainty caused by possible vertical air motions.

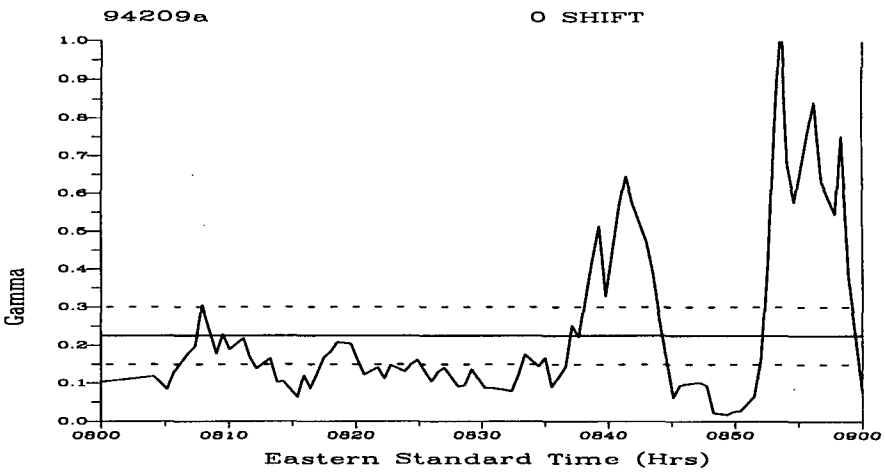


FIG. 6. The parameter $\gamma$ for case 2.

velocities in the rain are here greater than 8 m s$^{-1}$. These data were obtained with the regular pulse length of 0.7 $\mu$s and a range resolution of 105 m. Again, only three beams were used, and the scanning cycle emphasized the vertical beam: 3V-S-3V-W. A complete cycle thus took approximately 4 min, during which there were six samples in the vertical.

## 4. Analysis based on reflectivity and mean Doppler velocity

This approach makes use of (5), the relation between reflectivities and mean Doppler fallspeeds that follows from the assumption of a steady state and a one-to-one relation between the snowflakes entering the melting layer and the raindrops leaving it. From the observations just above and just below the bright band, we calculate the dimensionless quantity $\gamma$, defined by

$$\gamma = \frac{Ze_S\overline{v_S}}{Ze_R\overline{v_R}}, \tag{6}$$

where $\overline{v_S}$ and $\overline{v_R}$ are the measured mean downward velocities in the snow spectrum and the rain spectrum. These will differ from $\langle v_S\rangle$ and $\langle v_R\rangle$, if vertical air motions are present, and are given by

$$\left.\begin{aligned}\overline{v_S} &= \langle v_S\rangle - w_S\\ \overline{v_R} &= \langle v_R\rangle - w_R\end{aligned}\right\}, \tag{7}$$

where $w_S$ and $w_R$ are the updraft velocities in the snow and rain, respectively. Therefore, (6) becomes

$$\gamma = \frac{Ze_S(\langle v_S\rangle - w_S)}{Ze_R(\langle v_R\rangle - w_R)}. \tag{8}$$

If all the assumptions leading to (5) are satisfied (no growth, breakup, or vertical air motion), we should find that $\gamma = \mu = 0.23$. However, $\gamma$ may differ from $\mu$ if any of the assumptions are not satisfied. For example, if vertical air motions are negligible but particle growth by accretion or aggregation is significant, it will increase both $Ze_R$ and $\langle v_R\rangle$ and hence make $\gamma$ less than $\mu$. Conversely, breakup will make $\gamma$ larger than $\mu$. If vertical air motions may be neglected, the value of $\gamma$ may thus be used as a simple indicator of whether growth or breakup processes are significant in the melting layer and, if so, which is dominant. It is conceivable, of course, that growth and breakup could both be occurring in just the right proportion so that their opposite effects on $\gamma$ balance out.

To calculate $\gamma$ requires identifying an altitude just above the melting layer that represents the snow before melting and another altitude below the melting layer where the snow has changed to rain. These altitudes should be close together to minimize the time delay between the entry of the snow and the emergence of the rain, during which the advection of horizontal variations in the echo structure may affect the observations, but still far enough from the melting layer to ensure that the observations at the "snow" altitude are unaffected by melting and those at the "rain" altitude are unaffected by the ice phase. We identified these altitudes using an algorithm based on the vertical profile of reflectivity, as illustrated in Fig. 4. First, the top and bottom of the melting layer are defined as the levels of maximum curvature of the reflectivity profile above and below the reflectivity maximum, subject to the requirement that the levels are between 200 and 500 m from the reflectivity maximum. Then the reference levels for computing $\gamma$ are taken as one range increment (in this case 60 m) above the top and one range increment below the bottom of the melting layer. This procedure assures that the reference levels will be at least 260 m from the brightband peak, minimizing the chances of mixed phase precipitation at either level. So defined, the separation between the snow level and rain level is ordinarily about 600 m. The average fallspeed

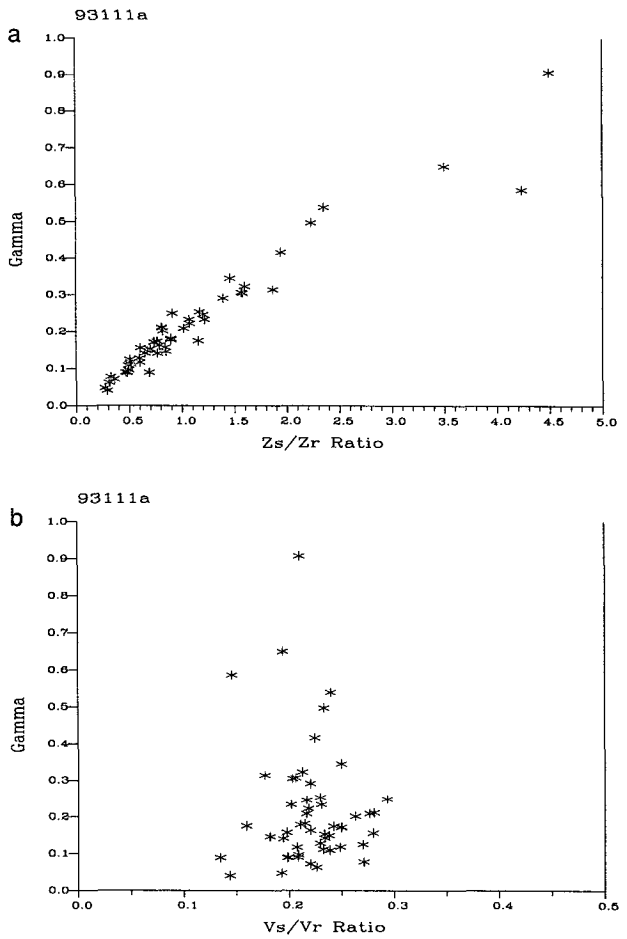


FIG. 7. The dependence of $\gamma$ in case 1 on (a) the ratio $Ze_S/Ze_R$ and (b) the ratio $v_S/v_R$.

over the vertical extent of the melting layer is about 4 m $s^{-1}$, so it takes a precipitation particle a time in the order of 2.5 min to fall through it.

Figure 5 shows $\gamma(t)$ for case 1. Before 1235 EST, $\gamma(t)$ lies generally below the value 0.23, implying that aggregation is the dominant process in the melting layer. Large values of $\gamma$ between 1240 and 1255 EST indicate breakup as the dominant process. After 1255, the values drop to the level indicating aggregation. Plotted also are two other curves of $\gamma(t)$: one with a time delay of 1 min between the measurements in snow and in rain, and the other with a delay of 2 min, to allow for time for the precipitation to fall from the snow level to the rain level. Although the curves differ slightly from one another because of time variations in the observed reflectivities and velocities, the interpretation of the data in terms of the dominant process in the melting layer is essentially the same, regardless of whether a time delay is considered. Basically, this is because the horizontal advection of spatial irregularities is generally unimportant for times up to 2 min or so. All further analysis is based on simultaneous observations, with no allowance for a time delay.

Figure 6 is $\gamma(t)$ for the data of case 2. Aggregation is indicated for times up to 0835 EST, after which there are two periods of approximately 5 min each in which $\gamma$ is considerably larger than 0.23, indicating the dominance of breakup.

Comparing Figs. 5 and 6 with the time height patterns in Figs. 1 and 3 shows that breakup tends to be associated with the passage of snow trails. More specifically, large values of $\gamma$ are explained by large values of the reflectivity ratio $Ze_S/Ze_R$. This is illustrated by Fig. 7a, a scatterplot of $\gamma$ versus the reflectivity ratio for the observations of 21 April 1993. An approximate linear dependence of $\gamma$ on $Ze_S/Ze_R$ is clearly indicated. That the reflectivity ratio is dominant in determining $\gamma$ is shown by Fig. 7b, a plot of $\gamma$ versus the velocity ratio for the same data sample. This shows that $\gamma$ is essentially independent of the velocity ratio. Hence, its variability is explained almost entirely by variability in the reflectivity ratio. Similar plots of the data in case 2 (not shown) give the same result.

We tentatively conclude from the evidence presented so far that aggregation is occurring much of the time, as indicated by values of $\gamma$ less than 0.23. In periods of heavy precipitation, however, breakup can become dominant and cause $\gamma$ to be greater than 0.23. Times when $\gamma \approx 0.23$ appear to be only transitions between the dominance of aggregation or breakup. To confirm this interpretation, we first consider the uncertainties in $\gamma$ caused by plausible vertical air motions and then examine the complete Doppler spectra in snow and rain, comparing them with the theoretical relation (4).

## 5. Effect of vertical air motions on $\gamma$

Until now, we have neglected the most significant potential source of error in data interpretation, namely,

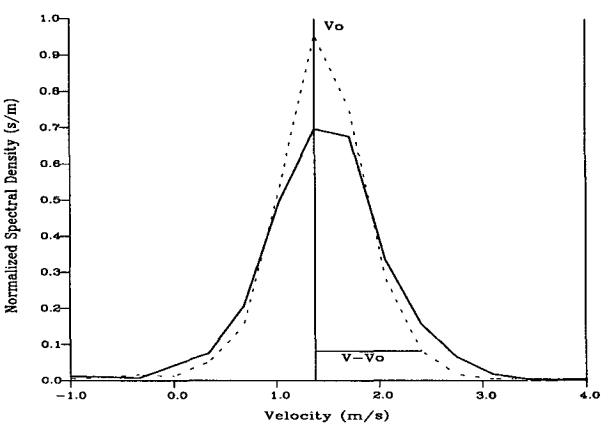


FIG. 8. Illustrating the approximate deconvolution operator (10). The solid curve is a measured spectrum. The dashed curve is the spectrum deconvolved to remove the spreading effect of a cross-beam wind of 11.5 m $s^{-1}$.

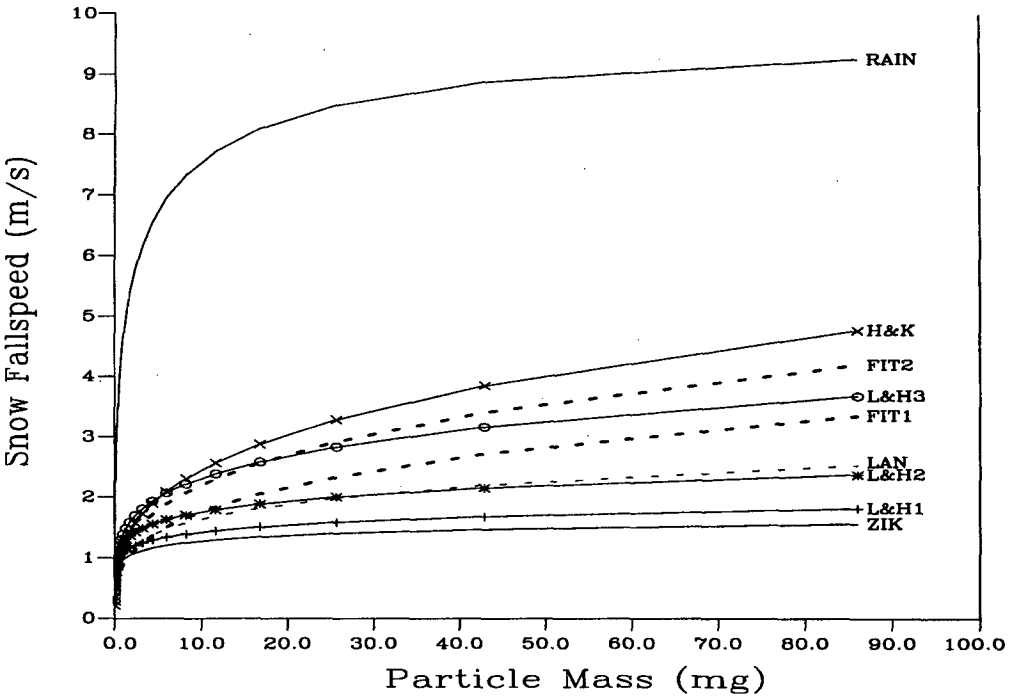


FIG. 9. Fallspeed as a function of mass implied by different empirical relations for ice-form precipitation listed in Table 1. The relation for rain is included for comparison.

updrafts and downdrafts. Their effect on $\gamma$ may be analyzed by assuming (5) and rearranging (8) to the form

$$\gamma = \mu \frac{\langle v_S \rangle - w_S}{\langle v_S \rangle - \rho w_R}, \tag{9}$$

where $\rho = \langle v_S \rangle / \langle v_R \rangle$. Typically, $\langle v_S \rangle \approx 1.5$ m s$^{-1}$ and $\rho \approx 1/4$. Using these values in (9) enables us to estimate the effect of updrafts on the parameter $\gamma$. For example, if $w_S = 0$ and $w_R = \pm 1$ m s$^{-1}$, $\gamma$ ranges between 0.19 and 0.27. Alternatively, if $w_R = 0$ and $w_S = \pm 0.5$ m s$^{-1}$, $\gamma$ varies between the broader limits of 0.15 and 0.30. The patterns of mean downward velocity in Figs. 1 and 3 are fairly smooth, suggesting that the variations in vertical air velocity are no greater than the values assumed in these examples. Hence, we may say that any observed values of $\gamma$ between approximately 0.15 and 0.30 are consistent with the assumptions of no growth or breakup, when allowance is made for plausible vertical air motions. These intervals are indicated on the plots of Figs. 5 and 6. Allowing for this uncertainty in $\gamma$ does not change the tentative conclusions given earlier.

## 6. Details for spectral comparisons

Two additional steps are required before we can employ (4) to compare the complete Doppler spectra in rain and snow. First, it is necessary to correct the measured spectra for the contribution of the cross-beam wind to the spectral spread. Second, the dependence of fallspeed on particle size must be specified to evaluate $dv_R/dv_S$ in (4).

### *a. Allowance for cross-beam wind*

Equation (4) assumes that the Doppler spectra are determined entirely by reflectivity-weighted particle fallspeeds. The measured spectra in the vertical profiler beam do indicate the distribution of fallspeed in the contributing volume but are broadened by turbulence and by the cross-beam (horizontal) wind component. We neglect turbulence in this analysis but apply an approximate correction to the measured spectra to remove the contribution of the cross-beam wind. Hitschfeld and Dennis (1956) showed that the cross-beam wind increases the spectral variance by an amount given by $\sigma_w^2 = 0.09\theta^2 V^2$, where $\theta$ is the beamwidth in radians and $V$ is the cross-beam wind component. For a vertical beam, $V$ is the horizontal wind speed, which is measured by the profiler.

To remove this contribution requires spectral deconvolution. The measured spectrum $S_0$, with variance $\sigma_0^2$, is deconvolved with the approximately Gaussian spread function of the cross-beam wind to yield the narrower spectrum $S$, with variance $\sigma^2 = \sigma_0^2 - \sigma_w^2$. We approximate the deconvolution by a "shrinking" operation defined by

$$S(v) = \frac{\sigma_0}{\sigma} S_0\left(v_0 + \frac{\sigma_0}{\sigma}(v - v_0)\right), \tag{10}$$

TABLE 1. Different fallspeed—diameter relations examined and shown in Fig. 9.

| Author | Particle type | $v_{s-D}$ relation | $m-D$ relation |
|---|---|---|---|
| Zikmunda (ZIK) | aggregates of radiating assemblages of dendrites | $v_s = 105 + 43 \log D$ (cm s$^{-1}$) (cm) | $m = 0.073\ D^{1.4}$ (mg) (mm) |
| Locatelli and Hobbs (L&H1) | aggregates of unrimed radiating assemblages of dendrites | $v_s = 0.81\ D^{0.16}$ (m s$^{-1}$) (mm) | $m = 0.073\ D^{1.4}$ (mg) (mm) |
| Locatelli and Hobbs (L&H2) | aggregates of densely rimed radiating assemblages of dendrites | $v_s = 0.79\ D^{0.27}$ (m s$^{-1}$) (mm) | $m = 0.037\ D^{1.9}$ (mg) (mm) |
| Locatelli and Hobbs (L&H3) | aggregates of unrimed sideplanes; assemblages of plates, columns and bullets | $v_s = 0.69\ D^{0.41}$ (m s$^{-1}$) (mm) | $m = 0.037\ D^{1.9}$ (mg) (mm) |
| Langleben (LAN) | mixture of dendrites and aggregates of plates | $v_s = 3.66\ D^{0.611}$ * (m s$^{-1}$) (cm) | $m = (\pi/6)\rho_L D^3$ (g) (cm) |
| Best fit to observations 21 April 1993 (FIT1) | amended Langleben | $v_s = 5.76\ D^{0.9}$ * (m s$^{-1}$) (cm) | $m = (\pi/6)\rho_L D^3$ (g) (cm) |
| Best fit to observations 28 July 1994 (FIT2) | amended Langleben | $v_s = 7.21\ D^{0.9}$ * (m s$^{-1}$) (cm) | $m = (\pi/6)\rho_L D^3$ (g) (cm) |
| Heymsfield and Kajikawa (H&K) | radiating assemblages of dendrites | $v_s = 1.37\ D^{0.83}$ (m s$^{-1}$) (cm) | $m = 0.00153\ D^{2.68}$ (g) (cm) |

* Uses melted diameter, where $\rho_L$ is density of liquid water, 1 g cm$^{-3}$.

where $v_0$ is the modal value of $S_0$. This operation would be an exact deconvolution if both $S_0$ and the spread function were Gaussian. It is a reasonable approximation for Doppler spectra that are unimodal, bell-shaped curves, as is often the case.

The effect of this technique is illustrated in Fig. 8, in which the solid curve is the original spectrum and the dashed line represents the "squeezed" spectrum whose width has been reduced by the width due to the cross-beam wind.

### b. *Fallspeed–size relations*

To apply (4), we need to specify the dependence of $v_R$ on $v_S$, which is determined by the relationships between particle fallspeed and size for both rain and snow. For rain, we use (Atlas et al. 1973)

$$v_R(D) = A - Be^{-CD}, \qquad (11)$$

where $A = 9.65$ m s$^{-1}$, $B = 10.43$ m s$^{-1}$, and $C = 6$ cm$^{-1}$. For snow, we use power-law relations of the form (Langleben 1954)

$$v_S(D) = \alpha D^{\beta} \qquad (12)$$

and have experimented with different values of $\alpha$ and $\beta$. Although the mean velocities and reflectivities calculated using Langleben's formula for a mixture of dendrites and plates were of the correct order of magnitude, the widths of the resulting spectra were much narrower than those observed. In an attempt to broaden the calculated spectra, the values of $\alpha$ and $\beta$ were amended to improve the fit to the data. To compare our "best fit" relations with some published fallspeed–size relations, Fig. 9 shows our best fit curves for the first and second cases studies (FIT1 and FIT2). The other relations are identified in Table 1.

## 7. Computed versus measured snow spectra

Having corrected the spectrum of rain $S_R$ for the spread due to the cross-beam wind and having specified $dv_R/dv_S$, we can employ (4) to transform the observed reflectivity and spectrum of the rain to the reflectivity and spectrum implied for the snow by the assumption that each raindrop was produced by a snowflake of the same mass. Figure 10 shows three examples. Each compares a computed snow spectrum (in heavy outline) with the one measured at the same time and corrected for the cross-beam wind. The first example is from case 2 at 0810 EST. The observed and computed reflectivities agree very closely, as do the mean Doppler fallspeeds. The agreement of spectral shapes is fairly close, though the computed spectrum has a standard deviation less than the measured one. Note for this case that the measured value of the parameter $\gamma$ is 0.19, hence within the window regarded as consistent with the assumptions of the simple transformation model. The second example is from case 2 at the later time of 0831 EST. Here, the computed reflectivity exceeds the measured value by 3 dBZ, and the computed and measured spectra are distinctly different from each other.

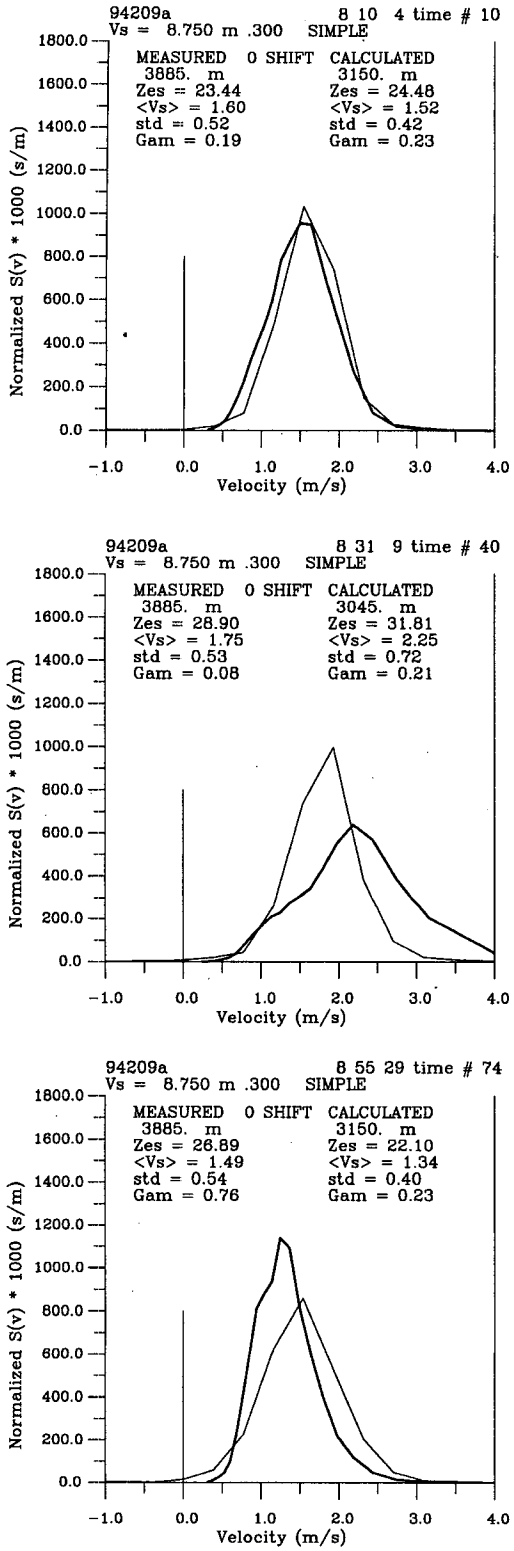


FIG. 10. Three examples from case 2 of measured snow spectra (light) compared with those derived from rain spectra (bold). Each frame includes the reflectivity, mean Doppler velocity, standard deviation, and $\gamma$ as determined from both the measured spectrum and the computed spectrum.

Significantly, the measured value of $\gamma$ is 0.08, indicating aggregation. The spectral misfit is consistent with this interpretation. The computed fall velocities in snow are greater than those measured because the drops in the rain spectrum are larger than implied by the snowflakes entering the melting layer. The last example is from the same dataset at 0855. In this case the computed spectrum is shifted to the left of the measured spectrum, which can be interpreted as arising from breakup, and is consistent with the large value of $\gamma$.

The simple transformation model can be modified to approximate, in a crude way, the effects of aggregation or breakup. To do this, we must recast the relations given earlier in terms of masses of the particles. The Doppler spectrum of the rain may be written

$$S_R(v_R)dv_R = \frac{Q_R(m_R)\epsilon^2 m_R^2 dm_R}{Ze_R}, \qquad (13)$$

where $m_R$ is the mass of a raindrop, $Q_R(m_R)dm_R$ is the size distribution in terms of mass, and $\epsilon = 6/\pi\rho$ with $\rho$ the density of water. The mass of the raindrop is determined by its velocity through the particle fall-speed–size relation for rain. Similarly, the Doppler spectrum of the snow may be written

$$S_S(v_S)dv_S = \frac{\mu Q_S(m_S)\epsilon^2 m_S^2 dm_S}{Ze_S}, \qquad (14)$$

where $m_S$ is the mass of a snowflake and $Q_S(m_S)dm_S$ is the size distribution in terms of mass. The mass distributions are related by

$$Q_S(m_S) = \frac{v_R(m_R)}{v_S(m_S)} Q_R(m_R). \qquad (15)$$

The simple model assumes a one-to-one relation between the snowflakes and raindrops such that the mass of a snowflake equals the mass of the raindrop and there are as many snowflakes as raindrops. Aggregation may be approximated by assuming that each raindrop of mass $m$ was created by the coalescence of two wet snowflakes of mass $m/2$ each. To satisfy conservation of mass, there must be twice as many snowflakes of mass $m_S = \frac{1}{2}m_R$ as raindrops of mass $m_R$. Replacing $m_S$ in (14) and (15) by its $m_R$ equivalent and combining with (13) leads to

$$S_S(v_S) = \frac{1}{4}\mu \frac{Ze_R v_R(m_R)}{Ze_S v_S(m_S)} S_R(v_R) \frac{dv_R}{dv_S} \qquad (16)$$

as the approximation for aggregation, where $m_S = \frac{1}{2}m_R$. Conversely, breakup is approximated by assuming that each snowflake of mass $2m$ breaks to form two raindrops of mass $m$ each. Hence, this model assumes that there are only half as many snowflakes of mass $m_S = 2m_R$ as raindrops of mass $m_R$. Performing the same substitutions as above yields

$$S_S(v_S) = 4\mu \frac{Ze_R v_R(m_R)}{Ze_S v_S(m_S)} S_R(v_R) \frac{dv_R}{dv_S} \qquad (17)$$

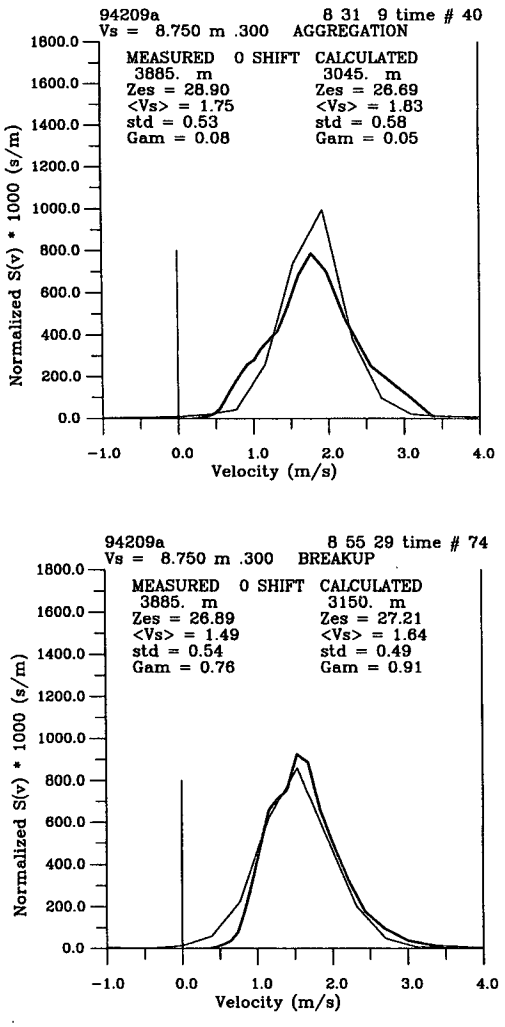


FIG. 11. Showing improved agreement in the lower two examples of Fig. 10 by employing models for aggregation (top) and breakup (bottom).

as the approximation for breakup, where $m_S = 2m_R$. These approximations were used for the examples in Fig. 10, and results are shown in Fig. 11. Not only do the modifications shift the computed spectra in the right direction for better agreement with observations, the computed reflectivities of the snow are brought into closer accord with observations. In short, any one of three transformation models—simple, aggregation, or breakup—may be used to calculate the snow spectrum from a given rain spectrum. Using $\gamma$ as a guide to the choice of model produces the best agreement between observed and computed spectra. However, it should be noted that the improvement in agreement is not always as good as in these examples.

## 8. Conclusions

We have shown that a measurable quantity, denoted by $\gamma$ and based on the radar reflectivities and mean Doppler velocities above and below the bright band, may be used as an indicator of the occurrence and the relative importance of aggregation and breakup processes in the melting layer. This interpretation is supported by comparison of the complete Doppler spectra measured above and below the bright band. The tentative conclusion is that aggregation occurs much of the time but that breakup effects may dominate when the rate of precipitation is sufficiently high.

*Acknowledgments.* This work was supported by grants from the U.S. Office of Naval Research and the Atmospheric Environment Service of Canada.

REFERENCES

Atlas, D., R. C. Srivastava, and R. S. Sekhon, 1973: Doppler radar characteristics of precipitation at vertical incidence. *Rev. Geophys. Space Phys.*, **2,** 1–35.

Austin, P. M., and A. C. Bemis, 1950: A quantitative study of the "bright band" in radar precipitation echoes. *J. Meteor.*, **7,** 145–151.

Dennis, A. S., and W. Hitschfeld, 1990: Advances in precipitation physics following the advent of weather radar. *Radar in Meteorology,* D. Atlas, Ed., Amer. Meteor. Soc., 98–108.

Drummond, F. J., 1994: Spectral interpretation of the melting layer using a wind profiler. M.S. thesis, Dept. of Atmospheric and Oceanic Sciences, McGill University, 97 pp. [Available from the Department of Atmospheric and Oceanic Sciences, McGill University, Montreal H3A 2K6, PQ, Canada.]

Ekpenyong, B., and R. C. Srivastava, 1970: Radar characteristics of the melting layer—A theoretical study. Preprints, *14th Conf. on Radar Meteorology,* Tucson, AZ, Amer. Meteor. Soc., 161–166.

Fabry, F., and I. I. Zawadzki, 1995: Long-term radar observations of the melting layer of precipitation and their interpretation. *J. Atmos. Sci.*, **52,** 838–851.

Gunn, K. L. S., and J. S. Marshall, 1958: The distribution with size of aggregate snowflakes. *J. Meteor.*, **15,** 452–461.

Hitschfeld, W., and A. S. Dennis, 1956: Measurement and calculation of fluctuations in radar echoes from snow. McGill University Stormy Weather Group, Scientific Rep. MW-23, 50 pp. [Available from Department of Atmospheric and Oceanic Sciences, McGill University, Montreal H3A 2K6, PQ, Canada.]

Klaassen, W., 1988: Radar observations and simulations of the melting layer of precipitation. *J. Atmos. Sci.*, **45,** 3741–3753.

Langleben, M. P., 1954: The terminal velocity of snowflakes. *Quart. J. Roy. Meteor. Soc.*, **80,** 174–181.

Rogers, R. R., S. A. Cohn, W. L. Ecklund, J. S. Wilson, and D. A. Carter, 1990: Experience from one year of operating a boundary-layer profiler in the center of a large city. *Ann. Geophys.*, **12,** 529–540.

Ryde, J. W., 1946: The attenuation and radar echoes produced at centimetre wave-lengths by various meteorological phenomena. *Meteorological Factors in Radio Wave Propagation,* Physical Society, 169–189.

Smith, P. L., 1984: Equivalent radar reflectivity factors for snow and ice particles. *J. Climate Appl. Meteor.*, **23,** 1258–1260.

Willis, T. W., and A. J. Heymsfield, 1989: Structure of the melting layer in mesoscale convective system stratiform precipitation. *J. Atmos. Sci.*, **46,** 2008–2025.